A novel shape memory alloy damping inerter for vibration mitigation

Smart Mater. Struct. **28** (2019) 115002 (12pp) https://doi.org/10.1088/1361-665X/ab3dc8

A novel shape memory alloy damping inerter for vibration mitigation

Yingqi Jia, Lingzhi Li, Chao Wang, Zhoudao Lu and Ruifu Zhang

Department of Disaster Mitigation for Structures, Tongji University, Shanghai 200092, People's Republic of China

E-mail: zhangruifu@tongji.edu.cn

Received 27 March 2019, revised 26 June 2019
Accepted for publication 22 August 2019
Published 1 October 2019

Abstract

Various shape memory alloy (SMA) dampers have been developed to reduce structural vibration responses. However, the application of SMA dampers has been restricted by the high material costs of SMAs. Therefore, this study developed and tested an innovative SMA damping inerter (SDI) in which an SMA element and an inerter element were arranged in parallel and deployed in series with a supporting spring element. A single-degree-of-freedom structure with an SDI was employed to analyze the effect of vibration mitigation. A theoretical analysis was conducted via an equivalent linearization method, and parameter studies were then used to evaluate the performance of the SDI-fitted structure from perspectives of structural displacement, acceleration, and energy dissipation as well as the most efficient frequency tuning bandwidth. The performances of the SDI and a conventional SMA damper were compared by using a time-domain analysis with recorded and simulated ground motions, revealing clearly superior results for the SDI with respect to structural response mitigation, and seismic energy dissipation. The system proposed here took advantage of the full potential of combining SMA and inerter elements, making the SDI a robust system for mitigating structural vibration with more economical SMA material costs.

Keywords: inerter, structural vibration mitigation, dynamic analysis, shape memory alloy

(Some figures may appear in colour only in the online journal)

1. Introduction

Buildings are structurally vulnerable to earthquakes and other hazardous events. With rising building heights and disaster frequency, structural vibration control [1–14] and retrofit strategies [15, 16] have attracted increasing attention. Structural responses can be suppressed to a target level by employing supplemental active [17, 18], passive [1, 2, 12, 19–21], semi-active [22, 23], and hybrid control [24] devices. Recently, shape memory alloy (SMA) dampers [8–10, 13, 14] have been developed with the high-quality super-elasticity characteristic.

SMAs can be transformed from one phase to another when induced by temperature or stress, and their shape can recover to the initial state if the temperature or stress effect is removed. The residual deformation is negligible if the SMA is in austenite state, which is known as super-elasticity [25]. Flag-shaped hysteresis loops resulting from the phase transformation of microstructures can be formed when SMAs are under cyclic loading, representing the capacity of energy dissipation. In this regard, SMAs can be considered as a promising energy dissipation material [26]. For example, Araki *et al* [27, 28] proposed a super-elastic Cu-Al-Mn SMA tension, which employed SMA as an energy dissipating and self-centering element. Mishra *et al* [10] presented a tuned mass damper assisted by a single SMA element based on the phase transformation mechanism of SMAs. These systems can effectively suppress structural responses.

However, SMA dampers have not been widely employed in practical engineering, because the value of their seismic response mitigation is restricted due to high material costs. Moreover, conventional SMA dampers have a deficiency in their design theory. SMA dampers are devised to suppress structural responses such as the displacement, but the decrease in structural displacement is usually accompanied by a reduction in deformation of the SMA element, resulting in

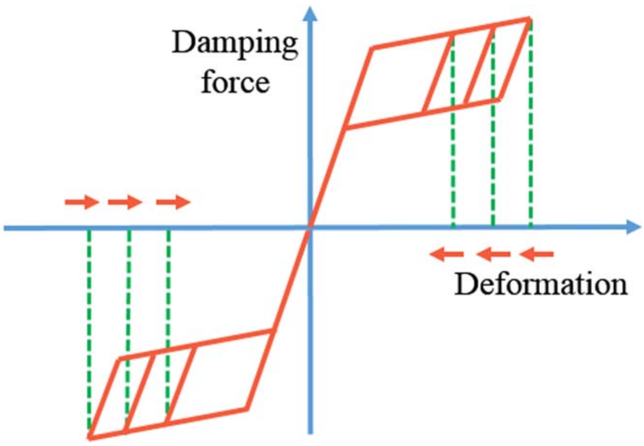

Figure 1. Hysteresis loops of SMA element.

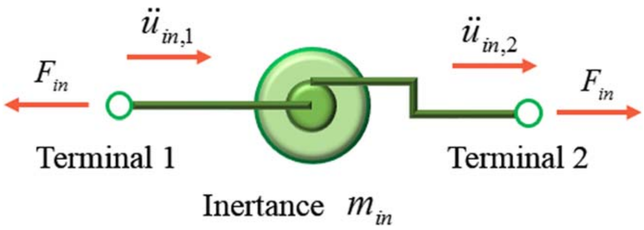

Figure 2. Two-terminal mechanical inerter element.

an insufficient hysteresis loop (figure 1). Therefore, the maximum potential of SMA elements has not been fully utilized in conventional SMA dampers, such that more SMAs are required to satisfy the same structural vibration mitigation requirement, raising the unnecessary cost.

To eliminate these structural displacement limitations in SMA elements, an innovative two-terminal mechanical element, referred as inerter element [1–5, 29–32] (figure 2), can be used. Unlike a classic mass element with a reaction force proportional to the absolute acceleration, the output force of an inerter element is given as [3]:

$$F_{in} = m_{in}(\ddot{u}_{in,2} - \ddot{u}_{in,1}), \tag{1}$$

where m_{in} represents the inertance of the inerter element. $\ddot{u}_{in,1}$ and $\ddot{u}_{in,2}$ are the accelerations of its two terminals, respectively (figure 2). In terms of implementation, ball-screw or rack-and-pinion mechanics are commonly utilized in an inerter element [3]. When relative displacement is exerted between the two terminal points, the ball screw rotates under the driving force, allowing the flywheel and tube to rotate with it. By this means, the additional mass is amplified owing to the rotational inertia of the flywheel, and damping effect can also be amplified (such as high-speed shearing between the tube and a viscous element connected to the inerter element [4]); the superior mass and damping enhancement effects of such inerter elements have been validated by many studies [1–5, 29, 30].

To improve the energy dissipation efficiency of SMA elements, this study proposed an innovative SMA damping inerter (SDI) system. The proposed system comprised an inerter element, an austenite SMA element, and a linear supporting spring. Owing to the mass and damping enhancement effects and the two-terminal connection characteristic of the inerter element, the hysteresis loop of the SMA element was not restricted by the displacement limitation. A single-degree-of-freedom (SDOF) structure with an SDI was employed to analyze the vibration mitigation effect, and the theoretical analysis was conducted via the equivalent linearization method. Then the parametrical analysis was used to investigate the damping effect and efficient tuning bandwidth for varying design parameters. The viability of the proposed system was further verified via time-domain analysis under recorded earthquake ground motions.

2. Outline of SDI system

2.1. Mechanical models

Two mechanical models of SDOF structures with and without the SDI are adopted for theoretical analysis (figure 3). The employed SDOF structure comprises the structural mass m, linear structural spring part k, and structural inherent damping c. In the proposed SDI system, an SMA element k_s and an inerter element m_{in} are arranged in parallel and deployed in series with a supporting spring k_d. When subjected to ground motions, the structural frequency can be tuned by the linear supporting spring. Meanwhile, the seismic input energy could be substantially dissipated by the SMA element, which is further enhanced by the inerter element. Thus, a robust structural vibration mitigation effect could be achieved by the interaction among the three elements. Considering that SMA wires might be buckled by compressive loads [33, 34], many attempts have been made by scholars to address this issue [9, 28, 35]. In these works, SMA wires in the SMA element are subjected in tensile strain all the time regardless of the moving direction of the primary structure. Therefore, the tension phase of SMA wires can be fully utilized no matter the SMA element is in tension or compression, and the buckling phenomenon of SMA wires could be avoided. Under this circumstance, the integrated hysteresis loop of SMA element in figure 1 could be realized. The notations used in this study are defined in table 1.

2.2. Phase transformation mechanism of the SMA

The SMA comprises two kinds of phases (austenite and martensite; the latter could be further classified to twinned martensite and detwinned martensite) and six kinds of crystal structures, with the capacity to transform from one phase to another under varying temperatures and loads [36]. With regard to the SMA beginning with 100% twinned martensite (figure 4(a)), the hysteretic curve is a classic bilinear model. From O to A (A′), the SMA is subjected to elastic deformation in the state of twinned martensite. The direction of the skeleton curve changes at point A (A′), which is analogous to the yield point of the steel. From A (A′) to B (B′) the displacement of the SMA increases substantially, and it is completely transformed into detwinned martensite at point B (B′). Unloading from point B (B′) to C (C′), a small part of the

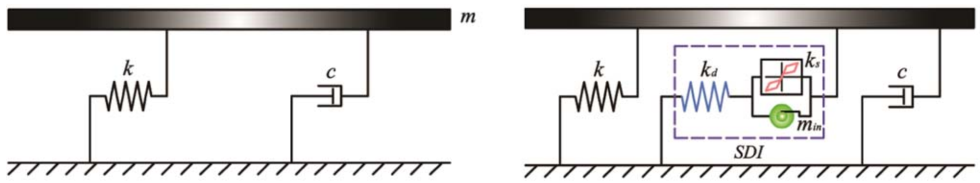

(a) SDOF structure without SDI (b) SDOF structure with SDI

Figure 3. Mechanical models of SDOF structures (a) without and (b) with the SDI.

strain is recovered; however, large-scale residual deformation remains even if the load is removed. Although the remaining residual strain can be fully recovered after heating the SMA, due to the shape memory effect [26], this property is not of interest in this study.

In terms of the SMA beginning with 100% austenite (figure 4(b)), the force-deformation curve clearly behaves as a double-flag-shaped hysteresis loop. The SMA is loaded along O-A-B-D (O-A′-B′-D′), transforming from austenite to detwinned martensite, and unloaded along D-C-A-O (D′-C′-A′-O′), transforming from detwinned martensite to austenite. Under the actions of circular loading and unloading, the hysteresis loop is formed and represents the energy dissipation capacity. There is little residual deformation when the load is removed, resulting from the super-elasticity of the SMA [26]. From the perspective of superior energy dissipation and negligible residual deformation, the austenite SMA can be regarded as an ideal element for SDI systems to mitigate structural vibration.

2.3. Constitutive model of the SMA element

As an essential part of the SDI system, the SMA element plays a vital role in seismic energy dissipation, so it is necessary to study its force-deformation behavior and establish the equations of motion. For this purpose, it is beneficial to give the mathematical constitutive model of the SMA element. The thermomechanical behavior of SMAs was well illustrated in Brinson's model [36], which accurately represented not only the super-elasticity but also the shape memory effect under all temperatures. However, Du *et al* [37] considered Brinson's model too complicated for practical use, instead presenting a simplified one-dimensional piecewise linear model based on Brinson's model. This model still requires solving a series of differential equations, which is difficult to apply to dynamic analysis of structures. In addition, the Graesser–Cozzaralli model [38] (based on the classic Bouc–Wen model [39]) can be used to describe the geometric shape of the constitutive relation curve of SMAs, in which the physical meanings of parameters are equivocal and the expressions are inevitably still in differential forms.

Yan and Nie [40] presented an improved model to facilitate the process of stochastic linearization. This model is widely employed for researching nonlinear dynamic characteristics of SMA-based systems [10], and is employed in this study for its concise expressions and explicit physical meanings. In this model, the restoring force of the SMA element can be expressed as [40]:

$$F_s = \alpha_s k_s x + (1 - \alpha_s) k_s z_s, \tag{2}$$

where α_s is the stiffness ratio of post- to pre-yielding, and x is the SMA displacement. The hysteretic part of the displacement z_s is given as:

$$z_s = [1 - \mathrm{sign}\{\mathrm{sign}(|x| - u_a) + 1\}]x + \frac{\mathrm{sign}(|x| - u_a) + 1}{2} \times \left[(u_b - u_a)\frac{\mathrm{sign}(x) + \mathrm{sign}(\dot{x})}{2} + u_a \mathrm{sign}(x)\right], \tag{3}$$

where u_a is the maximum displacement in the austenite phase, u_b is the displacement triggering martensitic transformation process, $\dot{x}$ represents the velocity of SMA element, and $\mathrm{sign}(x)$ is the mathematical sign function defined as:

$$\mathrm{sign}(x) = \begin{cases} 1, & \text{if } x > 0 \\ 0, & \text{if } x = 0. \\ -1, & \text{if } x < 0 \end{cases} \tag{4}$$

3. Equivalent linearization for nonlinear hysteresis of the SMA

Considering that hysteresis characteristic of SMA elements is highly nonlinear, it is beneficial to employ a convenient method to simplify the complicated force-deformation behavior of these elements. Among many analytical methods that have been developed to solve this kind of nonlinear problem [6, 40–43], the equivalent linearization method [40] is a promising tool from the perspective of conciseness with a wide range of solutions and is employed in this study. According to this method, the nonlinear system can be replaced by a linear system. Thus the equivalent form of equation (3) can be expressed as:

$$\bar{z}_s = k_e x + c_e \dot{x}, \tag{5}$$

where k_e and c_e are two stochastically equivalent terms.

Substituting equations (5) into (2), the equivalent form of the restoring force can be expressed as:

$$F_s = \alpha_s k_s x + (1 - \alpha_s) k_s (k_e x + c_e \dot{x}) = \tilde{k}_e x + \tilde{c}_e \dot{x}, \tag{6}$$

Table 1. Notations.

Notation	Definition
m	Structural mass
k	Structural stiffness
c	Structural inherent damping
m_{in}	Inertance of inerter element in SDI
k_s	Stiffness of SMA element in SDI
k_d	Stiffness of supporting spring in SDI
F_s	Restoring force of the SMA element
α_s	Stiffness ratio of post- to pre-yielding of SMA
x	Displacement of the SMA
z_s	Hysteretic part of the SMA displacement
u_a	Maximum displacement in the austenite phase of SMA
u_b	Displacement triggering martensitic transformation process of SMA
$\dot{x}$	Velocity of SMA
$\bar{z}_s$	Equivalent form of hysteretic part of the SMA displacement
k_e, c_e	Stochastically equivalent terms in equivalent linearization process
$\tilde{k}_e$, $\tilde{c}_e$	Stochastically equivalent stiffness and damping coefficients
σ_x, $\sigma_{\dot{x}}$	Standard deviations of displacement and velocity of SMA element
u_p, $\dot{u}_p$, $\ddot{u}_p$	Displacement, velocity and acceleration of primary structure
u_{in}, $\dot{u}_{in}$, $\ddot{u}_{in}$	Displacement, velocity and acceleration of inerter element
$\mathbf{u}$, $\dot{\mathbf{u}}$, $\ddot{\mathbf{u}}$	Displacement, velocity and acceleration vectors
$\mathbf{M}$, $\mathbf{C}$, $\mathbf{K}$	Mass, damping and stiffness matrices
S	Power spectral density filtered by Kanai–Tajimi model
ω	Filter frequency
S_0	Power spectral density of the rock
ω_g	Frequency of the soil strata
ζ_g	Damping of the soil strata
e_{total}	Total seismic-induced input energy
t	Time subjected to ground motion
$e_{k,p}$	Kinetic energy of primary structure
$e_{e,p}$	Elastic strain energy of primary structure
$e_{d,p}$	Energy dissipated by structural inherent damping
$e_{k,\mathrm{SDI}}$	Kinetic energy of SDI
$e_{e,\mathrm{SDI}}$	Elastic strain energy of SDI
$e_{d,\mathrm{SDI}}$	Energy dissipated by SDI
$\sigma_{\dot{u}_p}$	Standard deviation of the structural velocity
$\sigma_{z_s\dot{u}_{in}}$	Covariance of hysteretic part of the SMA displacement and velocity of inerter element
$\sigma_{u_{in}}$, $\sigma_{\dot{u}_{in}}$	Standard deviations of displacement and velocity of inerter element
μ	Ratio of inertance to structural mass
κ_s	Stiffness ratio of the SMA element to primary structure
κ_d	Stiffness ratio of supporting spring in SDI to primary structure
$\sigma_{u,\mathrm{ST-SDI}}$	Root-mean-square (RMS) displacement of the structure with SDI
$\sigma_{u,\mathrm{ST}}$	RMS displacement of the original structure
$\sigma_{a,\mathrm{ST-SDI}}$	RMS acceleration of the structure with SDI
$\sigma_{a,\mathrm{ST}}$	RMS acceleration of the original structure
γ_u	RMS displacement ratio of the structure with SDI to original structure
γ_a	RMS acceleration ratio of the structure with SDI to original structure
γ_E	Filtered energy ratio
w	Efficient bandwidth of frequency
T_p	Structural vibration period
ζ_p	Structural damping ratio

where $\tilde{k}_e$ and $\tilde{c}_e$ are stochastically equivalent stiffness and damping coefficients, respectively, which are given as:

$$\begin{cases} \tilde{k}_e = \alpha_s k_s + (1-\alpha_s) k_s k_e \\ \tilde{c}_e = (1-\alpha_s) k_s c_e \end{cases}. \tag{7}$$

To achieve an ideal equivalent linearization, the least square error between the linearized and nonlinear items $E[(\bar{z}_s - z_s)^2] = E[(k_e x + c_e \dot{x} - z_s)^2]$ should be satisfied. $E[\,]$ represents the expectation operator herein. Minimizing the least square error with respect to the stochastically equivalent terms k_e and c_e produces:

$$\frac{\partial[E(\bar{z}_s - z_s)^2]}{\partial k_e} = 0, \quad \frac{\partial[E(\bar{z}_s - z_s)^2]}{\partial c_e} = 0. \tag{8}$$

Equation (8) can be solved with respect to k_e and c_e as:

$$k_e = \frac{E[x \cdot z_s]}{E[x^2]}, \quad c_e = \frac{E[\dot{x} \cdot z_s]}{E[\dot{x}^2]}. \tag{9}$$

Substituting equations (3) in (9), k_e and c_e can be obtained as:

$$k_e = \frac{u_b + u_a}{\sqrt{2\pi}\,\sigma_x} \exp\left(-\frac{u_a^2}{2\sigma_x^2}\right), \quad c_e = \frac{u_b - u_a}{\sqrt{2\pi}\,\sigma_{\dot{x}}} \times \left[1 - \mathrm{erf}\left(\frac{u_a}{\sqrt{2}\,\sigma_x}\right)\right]. \tag{10}$$

where σ_x and $\sigma_{\dot{x}}$ are the standard deviations of x and $\dot{x}$, respectively, and $\mathrm{erf}(x)$ is the mathematical error function defined as:

$$\mathrm{erf}(x) = \frac{2}{\sqrt{\pi}} \int_0^x \mathrm{e}^{-\eta^2} d\eta. \tag{11}$$

Substituting equations (10) into (7), the stochastically equivalent stiffness $\tilde{k}_e$ and damping $\tilde{c}_e$ can be expressed as:

$$\begin{cases} \tilde{k}_e = \alpha_s k_s + (1-\alpha_s) k_s \dfrac{u_b + u_a}{\sqrt{2\pi}\,\sigma_x} \exp\left(-\dfrac{u_a^2}{2\sigma_x^2}\right) \\ \tilde{c}_e = (1-\alpha_s) k_s \dfrac{u_b - u_a}{\sqrt{2\pi}\,\sigma_{\dot{x}}} \left[1 - \mathrm{erf}\left(\dfrac{u_a}{\sqrt{2}\,\sigma_x}\right)\right] \end{cases}. \tag{12}$$

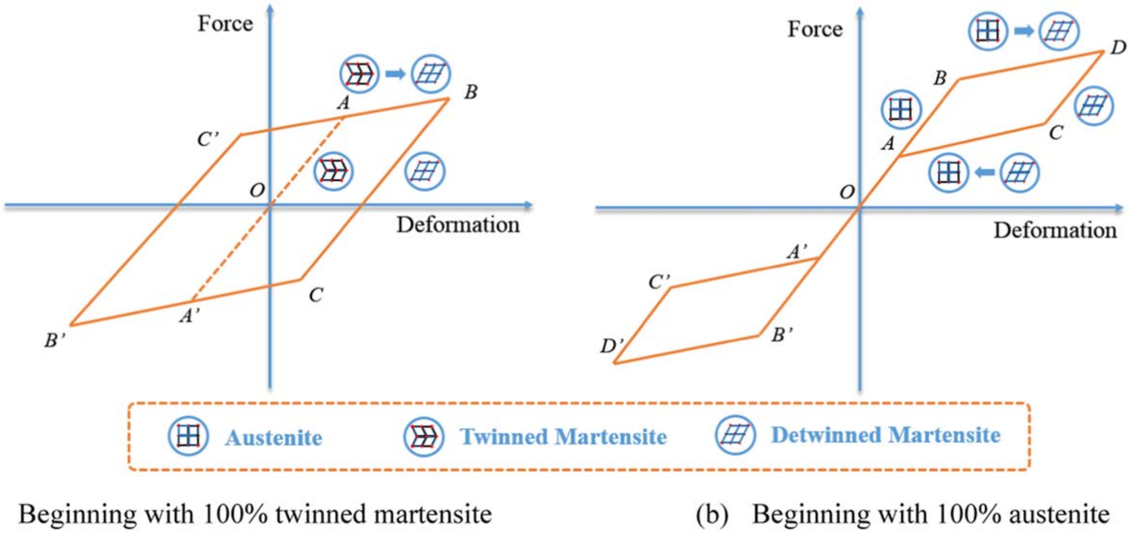

Figure 4. Schematic of force-deformation curves of SMAs beginning with (a) 100% twinned martensite and (b) 100% austenite.

4. Theoretical analysis

4.1. Equations of motion

According to equation (6), the damping force provided by the SMA element in the SDI comprises the two terms $\tilde{k}_e x$ and $\tilde{c}_e \dot{x}$, which are analogous to the contributions of a supporting spring $\tilde{k}_e$ and an energy dissipation element $\tilde{c}_e$, respectively. Therefore, the mechanical model of the SDOF structure with an SDI in figure 3(b) could be equivalent to a simplified form via the equivalent linearization method (figure 5). In contrast to figure 3(b), herein the SMA element is replaced by a supporting spring $\tilde{k}_e$ and an energy dissipation element $\tilde{c}_e$.

By the means of equivalent linearization, the motion-governing equations of the SDOF structure with an SDI subjected to a horizontal ground motion can be given as follows:

$$\begin{cases} m\ddot{u}_p + c\dot{u}_p + ku_p + k_d(u_p - u_{in}) = -m\ddot{u}_g \\ m_{in}\ddot{u}_{in} + \tilde{c}_e\dot{u}_{in} + \tilde{k}_e u_{in} = k_d(u_p - u_{in}) \end{cases}, \tag{13}$$

where u_p and u_{in} are the displacements of the primary structure and inerter element, respectively, with respect to the ground. The respective velocities and accelerations are denoted as $\dot{u}_p$, $\dot{u}_{in}$, $\ddot{u}_p$, and $\ddot{u}_{in}$. The ground acceleration of the earthquake is represented as $\ddot{u}_g$. Equation (13) can also be expressed in the matrix form as:

$$\mathbf{M}\ddot{\mathbf{u}} + \mathbf{C}\dot{\mathbf{u}} + \mathbf{K}\mathbf{u} = -\mathbf{M}\mathbf{r}\ddot{u}_g, \tag{14}$$

where $\mathbf{u} = \{u_p, u_{in}\}^T$, $\dot{\mathbf{u}} = \{\dot{u}_p, \dot{u}_{in}\}^T$ and $\ddot{\mathbf{u}} = \{\ddot{u}_p, \ddot{u}_{in}\}^T$ are the vectors of displacement, velocity, and acceleration, respectively, $\mathbf{r} = \{1, 0\}^T$ is the vector of influence coefficient, and $\mathbf{M}$, $\mathbf{C}$, and $\mathbf{K}$ are the mass, damping, and stiffness matrices, respectively, expressed as:

$$\mathbf{M} = \begin{bmatrix} m & \\ & m_{in} \end{bmatrix}, \quad \mathbf{C} = \begin{bmatrix} c & \\ & \tilde{c}_e \end{bmatrix}, \quad \mathbf{K} = \begin{bmatrix} k + k_d & -k_d \\ -k_d & k_d + \tilde{k}_e \end{bmatrix}. \tag{15}$$

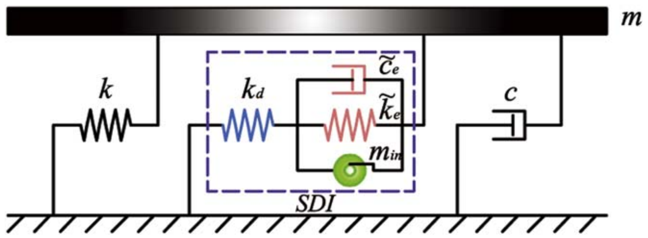

Figure 5. Simplified form of the SDOF system with an SDI.

To obtain the stationary ground motion, the well-known Kanai–Tajimi model [44] is employed to filter a white noise process acting at the rock bed:

$$S(\omega) = S_0 \frac{\omega_g^4 + 4\zeta_g^2\omega_g^2\omega^2}{(\omega_g^2 - \omega^2)^2 + 4\zeta_g^2\omega_g^2\omega^2}, \tag{16}$$

where $S(\omega)$ is the power spectral density filtered by the Kanai–Tajimi model, ω is the filter frequency, S_0 is the power spectral density of the rock, and ω_g and ζ_g are the frequency and damping of the soil strata, respectively.

4.2. Energy balance analysis

Regarding the energy-based evaluation, seismic-induced input energy is dissipated by not only the primary structure but also the SMA element in the SDI. From the perspective of time-domain analysis, the energy balance equation is given as follows:

$$\begin{aligned} e_{total}(t) = e_{k,p}(t) + e_{e,p}(t) + e_{d,p}(t) + e_{k,\mathrm{SDI}}(t) \\ + e_{e,\mathrm{SDI}}(t) + e_{d,\mathrm{SDI}}(t), \end{aligned} \tag{17}$$

where $e_{total}(t)$ is total seismic-induced input energy, t represents the time subjected to ground motion, $e_{k,p}(t)$, $e_{e,p}(t)$ and $e_{d,p}(t)$ are the structural kinetic energy, elastic strain energy, and energy dissipated by structural inherent damping, respectively, and $e_{k,\mathrm{SDI}}(t)$, $e_{e,\mathrm{SDI}}(t)$ and $e_{d,\mathrm{SDI}}(t)$ are the respective counterparts for the SDI. For the sake of seismic-induced input

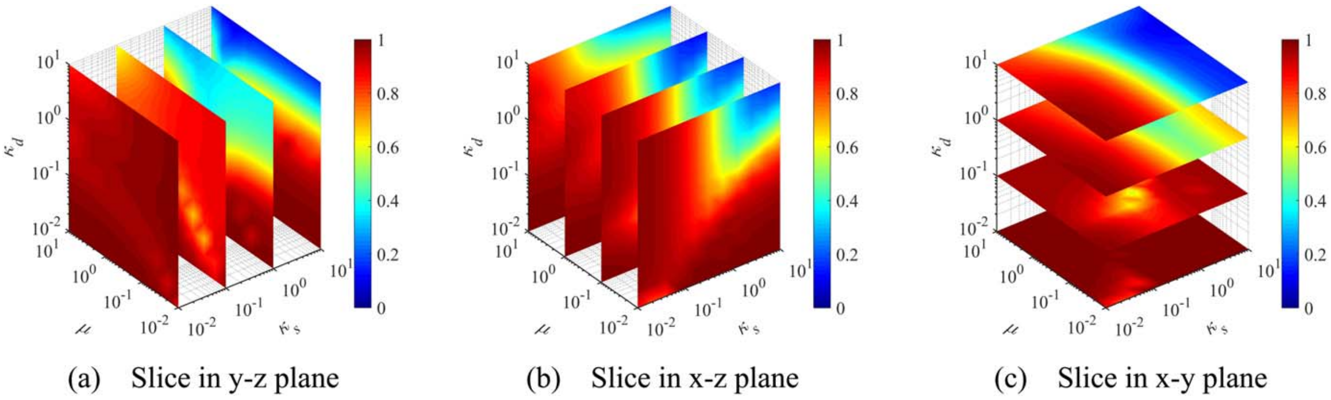

Figure 6. Slice figures of the displacement ratios γ_u for μ, κ_s, and $\kappa_d \in [10^{-2}, 10^1]$.

energy being a stochastic process, the energy response should be investigated stochastically by applying an expectation operator $E[\,]$ to both sides of equation (17). Considering the stationarity hypothesis, we obtain:

$$E[e_{k,p}(t)] = E[e_{e,p}(t)] = E[e_{k,\mathrm{SDI}}(t)] = E[e_{e,\mathrm{SDI}}(t)] = 0. \tag{18}$$

In addition, the damping-dissipated energy of primary structure $e_{d,p}(t)$ and SDI $e_{d,\mathrm{SDI}}(t)$ can be expressed as follows:

$$\begin{cases} e_{d,p}(t) = \int_0^t c\dot{u}_p{}^2(\tau)d\tau \\ e_{d,\mathrm{SDI}}(t) = \int_0^t F_s\dot{u}_{in}(\tau)d\tau \\ \quad = \int_0^t [\alpha_s k_s u_{in}(\tau) + (1-\alpha_s)k_s z_s(\tau)]\dot{u}_{in}(\tau)d\tau \end{cases}. \tag{19}$$

Thus, the stochastically expected form of equation (17) can be written as:

$$\begin{aligned} E[e_{total}(t)] &= E[e_{d,p}(t)] + E[e_{d,\mathrm{SDI}}(t)] = E\left[\int_0^t c\dot{u}_p{}^2(\tau)d\tau\right] \\ &+ E\left[\int_0^t [\alpha_s k_s u_{in}(\tau) + (1-\alpha_s)k_s z_s(\tau)]\dot{u}_{in}(\tau)d\tau\right] \\ &= c\sigma_{\dot{u}_p}^2 + (1-\alpha)k_s\sigma_{z_s\dot{u}_{in}}, \end{aligned} \tag{20}$$

where $\sigma_{\dot{u}_p}$ is the standard deviation of the structural velocity $\dot{u}_p$, and $\sigma_{z_s\dot{u}_{in}}$ is the covariance of z_s in equation (3) and the velocity of the inerter element $\dot{u}_{in}$. Considering that $\dot{u}_{in}$ and z_s obey the normal distribution with a mean value equal to zero results in:

$$\begin{aligned} \sigma_{z_s\dot{u}_{in}} &= \frac{u_b - u_a}{2}\int_{-\infty}^{+\infty}\frac{\mathrm{sign}(|u_{in}| - u_a) + 1}{2\sqrt{2\pi}\,\sigma_{u_{in}}}\exp\left(-\frac{u_{in}^2}{2\sigma_{u_{in}}^2}\right) \\ &\times \mathrm{d}u_{in}\int_{-\infty}^{+\infty}\frac{\dot{u}_{in}\mathrm{sign}(\dot{u}_{in})}{\sqrt{2\pi}\,\sigma_{\dot{u}_{in}}}\exp\left(-\frac{\dot{u}_{in}^2}{2\sigma_{\dot{u}_{in}}^2}\right)\mathrm{d}\dot{u}_{in} \\ &= \frac{u_b - u_a}{\sqrt{2\pi}}\left[1 - \mathrm{erf}\left(\frac{u_a}{\sqrt{2}\,\sigma_{u_{in}}}\right)\right]\sigma_{\dot{u}_{in}}, \end{aligned} \tag{21}$$

where $\sigma_{u_{in}}$ and $\sigma_{\dot{u}_{in}}$ are the standard deviations of the displacement u_{in} and the velocity $\dot{u}_{in}$ of the inerter element, respectively.

Substituting equations (21) into (20), the expected value of total seismic-induced input energy can be given as:

$$E[e_{total}(t)] = c\sigma_{\dot{u}_p}^2 + (1-\alpha)k_s\frac{u_b - u_a}{\sqrt{2\pi}}\left[1 - \mathrm{erf}\left(\frac{u_a}{\sqrt{2}\,\sigma_{u_{in}}}\right)\right]\sigma_{\dot{u}_{in}}. \tag{22}$$

5. Parametric study

5.1. Stochastic performance indicators

To evaluate the effect of structural vibration mitigation for the SDI, four stochastic performance indicators are introduced. First, three dimensionless parameters (inertance-mass ratio μ, stiffness ratio κ_s, and linear stiffness ratio κ_d) widely used in seismic mitigation theories [3, 10] can be restated as:

$$\mu = m_{in}/m, \quad \kappa_s = k_s/k, \quad \kappa_d = k_d/k. \tag{23}$$

Two design indices can then be adopted: γ_u, the root-mean-square (RMS) displacement ratio of the structure with SDI $\sigma_{u,\mathrm{ST-SDI}}$ to the original structure $\sigma_{u,\mathrm{ST}}$, and γ_a, the ratio of the RMS acceleration of the structure with SDI $\sigma_{a,\mathrm{ST-SDI}}$ to the structure without SDI $\sigma_{a,\mathrm{ST}}$. These can be expressed as follows:

$$\gamma_u = \frac{\sigma_{u,\mathrm{ST-SDI}}}{\sigma_{u,\mathrm{ST}}}, \quad \gamma_a = \frac{\sigma_{a,\mathrm{ST-SDI}}}{\sigma_{a,\mathrm{ST}}}. \tag{24}$$

Considering that an energy-based performance index is more robust than γ_u and γ_a, which are displacement- and acceleration-based indices, a filtered energy ratio γ_E can also be utilized as:

$$\gamma_E = \frac{E[e_{total}(t)] - E[e_{d,\mathrm{SDI}}(t)]}{E[e_{total}(t)]}. \tag{25}$$

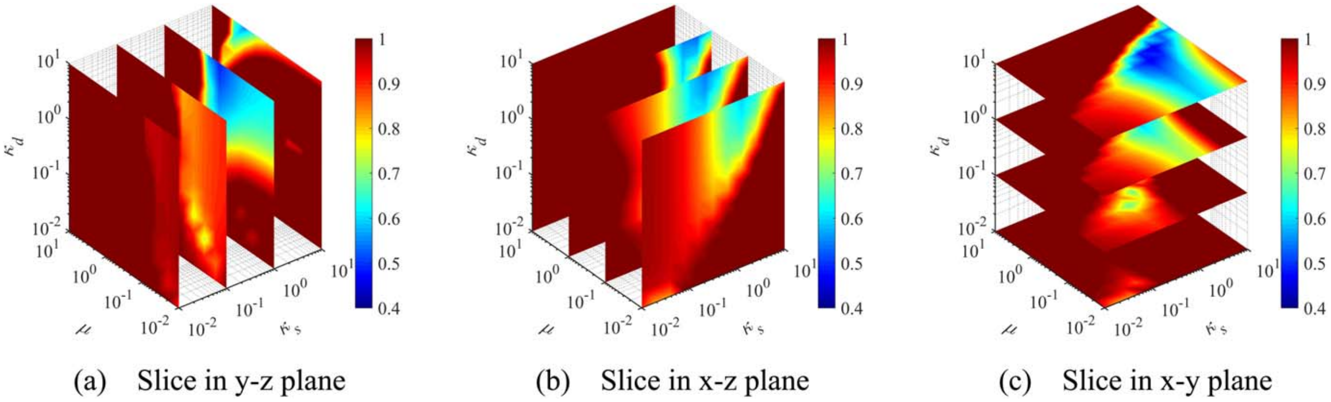

Figure 7. Slice figures of the acceleration ratios γ_a for μ, κ_s, and $\kappa_d \in [10^{-2}, 10^{1}]$.

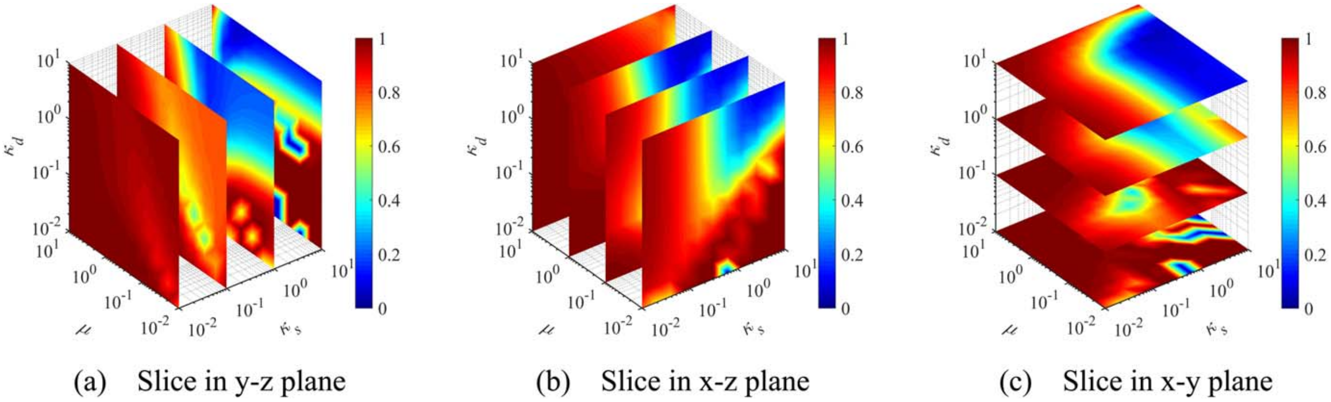

Figure 8. Slice figures of the filtered energy ratios γ_E for μ, κ_s, and $\kappa_d \in [10^{-2}, 10^{1}]$.

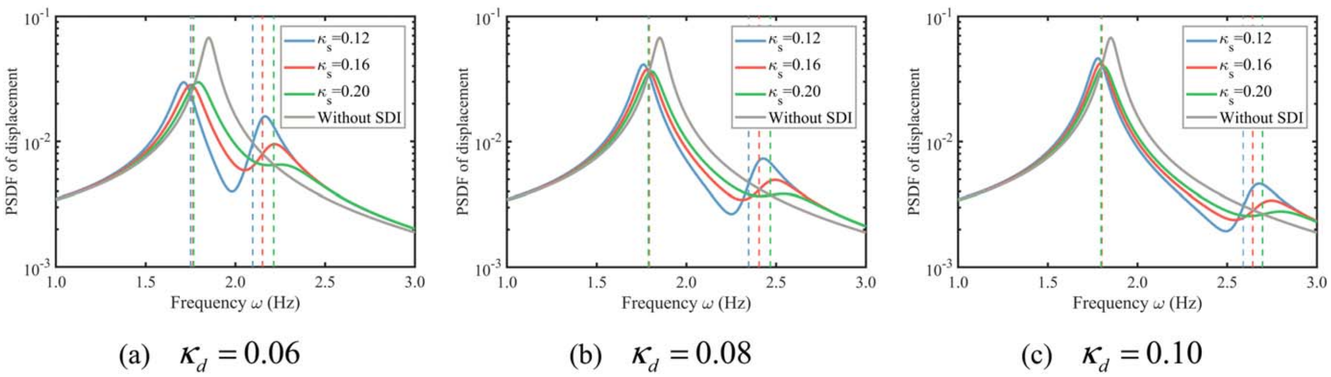

Figure 9. Displacement PSDFs of the SDOF structures with different SDI systems for $\mu = 0.06$, $\kappa_d \in [0.06, 0.10]$, and $\kappa_s \in [0.12, 0.20]$.

Referring back to equation (22), γ_E represents the proportion of the energy absorbed by the primary structure; a low γ_E value indicates a robust energy dissipation capacity of the SDI. Thus γ_E should also be taken into consideration. In addition, the efficient bandwidth of frequency w represents the robustness of the damping effect under seismic excitations with different frequency components, which should also be selected as a performance indicator. Hence, the parameter analytical problem can be summarized as follows:

$$\{\mu, \quad \kappa_s, \quad \kappa_d\} \rightarrow \{\gamma_u, \gamma_a, \gamma_E, w\}. \tag{26}$$

5.2. Seismic response mitigation effect

The parametric study employs a single-span and single-floor frame structure characterized by structural mass $m = 20 \times 10^3$ kg, vibration period $T_p = 0.54$ s, and structural damping ratio $\zeta_p = 0.02$ [45]. In the SDI system, $\alpha_s = 0.001$, $u_a = 0.005$ m, and $u_b = 0.02$ m are assumed for the SMA element [10]. $\zeta_g = 0.6$ and $\omega_g = 9\pi$ rad s^{-1} are selected as default values for the soil strata according to [10]. In addition, the reasonable range of the parameters of κ_s, μ, and κ_d are defined as $[10^{-2}, 10^{1}]$ to implement different control levels [3].

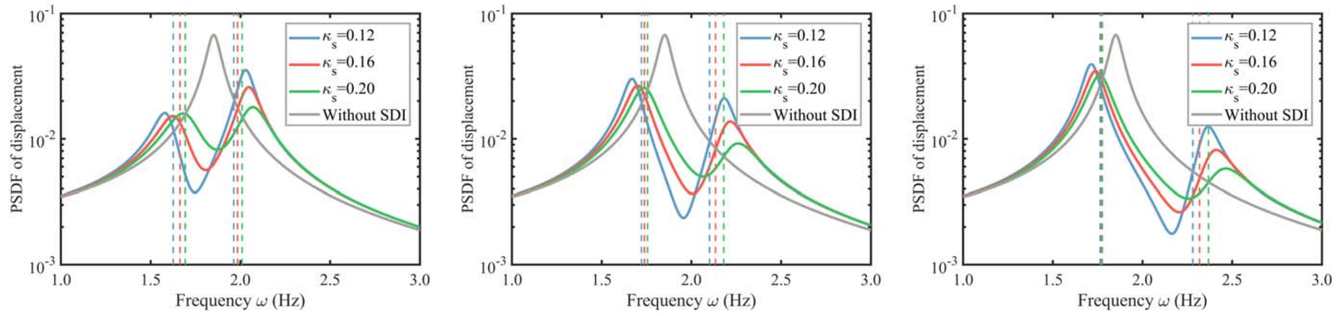

(a) $\kappa_d = 0.06$ (b) $\kappa_d = 0.08$ (c) $\kappa_d = 0.10$

Figure 10. Displacement PSDFs of the SDOF structures with different SDI systems for $\mu = 0.08$, $\kappa_d \in [0.06, 0.10]$, and $\kappa_s \in [0.12, 0.20]$.

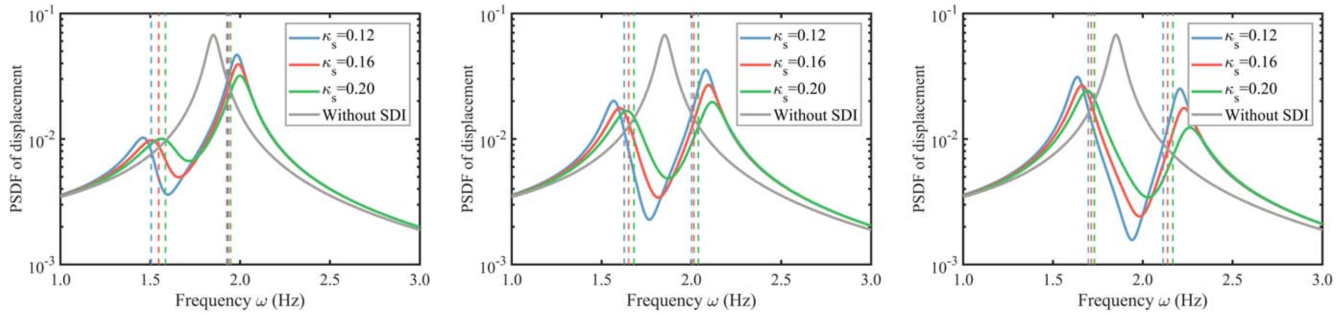

(a) $\kappa_d = 0.06$ (b) $\kappa_d = 0.08$ (c) $\kappa_d = 0.10$

Figure 11. Displacement PSDFs of the SDOF structures with different SDI systems for $\mu = 0.10$, $\kappa_d \in [0.06, 0.10]$, and $\kappa_s \in [0.12, 0.20]$.

Slice figures of RMS displacement ratio γ_u, acceleration ratio γ_a, and filtered energy ratio γ_E for different SDI systems are shown in figures 6–8. In each figure, the results are shown from three directions (y–z plane, x–z plane, and x–y plane). Moreover, κ_s, μ, and κ_d are on the *x*-, *y*-, and *z*-axis, respectively, and γ_u, γ_a, and γ_E are represented by the varying colors.

It could be observed from figure 6 that the acceptable displacement mitigation range is located in the upper-right corner (blue area). A decrease in γ_u is accompanied by increases in κ_s and κ_d (figures 6(a) and (c)), as a greater stiffness is imposed on the primary structure by the SMA element and linear supporting spring in the SDI. Moreover, the blue area can be quite wider when μ is in $[10^{-2}, 10^{0}]$ (figure 6(b)), indicating that an ideal displacement mitigation effect could be realized by an SDI with a lower SMA material cost.

For the acceleration ratio γ_a, the acceptable mitigation range is also located in the upper-right corner (blue area in figure 7). A value of κ_s in $[10^{-1}, 10^{0}]$ can be beneficial to the decrease in γ_a (figure 7(a)), whereas smaller μ and κ_d could do harm to the mitigation effect of the acceleration response (figures 7(b) and (c)), because the SMA element is poor at absorbing seismic energy in a timely manner without the assistance of inerter element and linear spring element.

The acceptable area of filtered energy ratio γ_E is the largest when μ is in $[10^{-2}, 10^{0}]$ (figure 8(b)). Under this circumstance, dissipating the substantial seismic input energy can be realized by an SDI with a smaller SMA material cost. Furthermore, increases in κ_s and κ_d can induce a dramatic decrease in γ_E (figures 8(a) and (c)), indicating less energy filtering into the primary structure while the SMA element in the SDI is absorbing most of the energy.

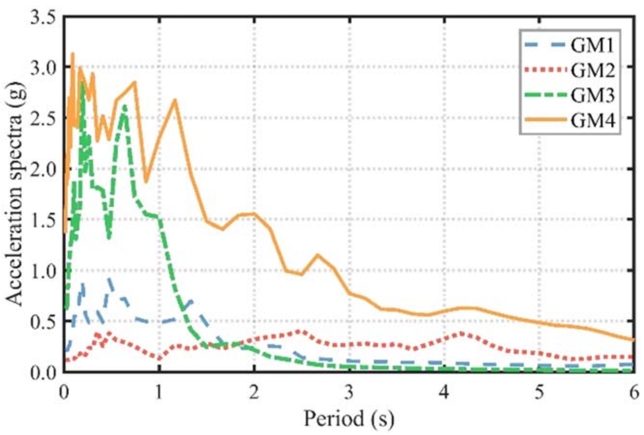

Figure 12. Acceleration spectra of input ground accelerations.

Based on the overall consideration of figures 6–8, the ideal parameter sets for acceptable seismic vibration mitigation effects are $\kappa_s \in [0.12, 0.20]$, $\kappa_d \in [0.06, 0.10]$, and $\mu \in [0.06, 0.10]$ based on these approximate estimates.

5.3. Efficient tuning bandwidth of frequency

To identify the efficient tuning bandwidth of frequency of the SDI system, the power spectral density functions (PSDFs) of

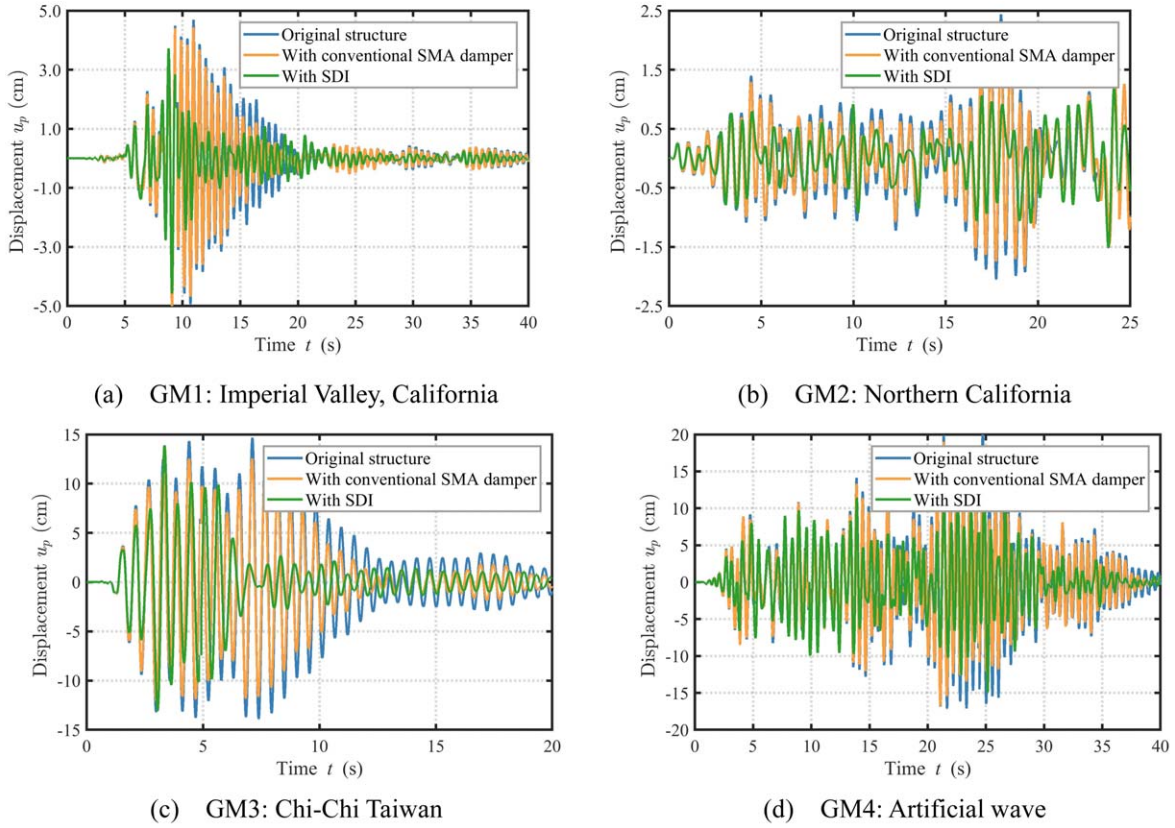

Figure 13. Time histories of displacements of primary structures' μ_p.

Table 2. Details of ground motions used for testing.

ID#	PGA (g)	Earthquake	Date	Station
GM1	0.212	Imperial Valley, California	10/15/1979	EC County Center FF
GM2	0.118	Northern California	11/22/1952	Ferndale City Hall
GM3	0.618	Chi-Chi Taiwan	9/20/1999	TCU115
GM4	1.043	Artificial wave	—	—

displacements of primary structures under the previously defined parameters are determined (figures 9–11). As the shape and tendency of the acceleration PSDF curves are similar to the displacement PSDFs, the former are not shown. Four observations can be made from these results. First, the efficient tuning bandwidth of frequency for the SDI increases with increasing κ_d, especially for smaller values of μ. Second, the efficient tuning bandwidth generally moves right with increasing κ_d, indicating that seismic energy with higher frequency components could be absorbed by the SDI system. Third, with smaller values of μ, efficient tuning bandwidth increases with increasing κ_s (figures 9 and 10), whereas the opposite occurs with larger values of μ (figure 11). Fourth, a decrease in the efficient tuning bandwidth is accompanied by an increase in μ. However, with increasing μ, the efficient tuning bandwidth moves left, and the left peak of the curves moves down while the right peak moves up. Thus, an optimal set for μ, κ_s, and κ_d exists according to the fixed point theory [4]. It is worthy to note that there are two degrees of freedom in the SDOF structures with the SDI, among which one degree of freedom is provided by the primary structure itself m, and the other one is generated by the inerter element m_{in}. Thus, it is reasonable for figures 9–11 to display one peak for structures without SDI and two peaks for structures with SDI.

6. Seismic performance

To further validate the structural vibration mitigation effect of the SDI, one artificial [46, 47] and three recorded ground motions are used for the time-domain analysis. For the sake of geographic representativeness, these acceleration records comprise different frequency components and are recorded by different stations. The details of the seismic waves are shown in table 2 and acceleration response spectra are shown in figure 12.

The design parameters for the SDI are set as $\mu = 0.08$, $\kappa_d = 0.08$, and $\kappa_s = 0.16$ (chosen from the above parametric analytical results). To assess the superiority of the SDI, an SMA damper with the same stiffness ($\kappa_s = 0.16$) is also

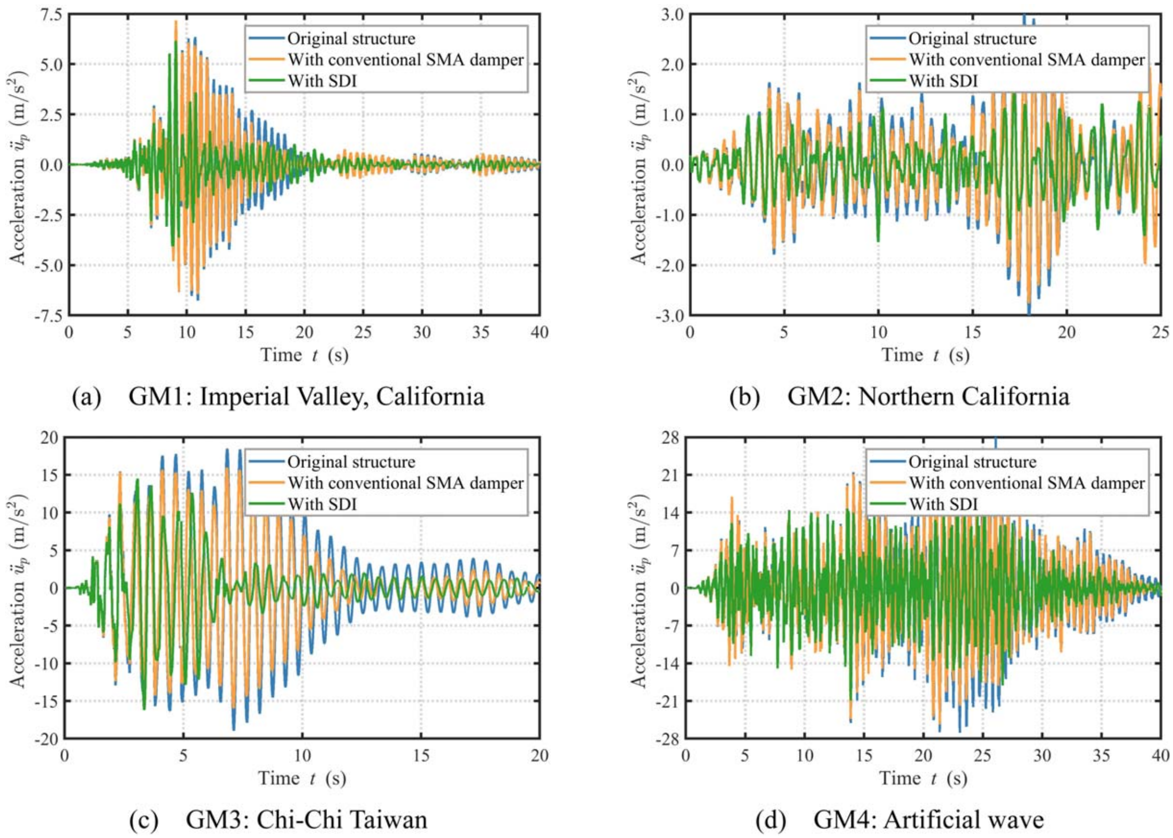

Figure 14. Time histories of accelerations of primary structures' $\ddot{u}_p$.

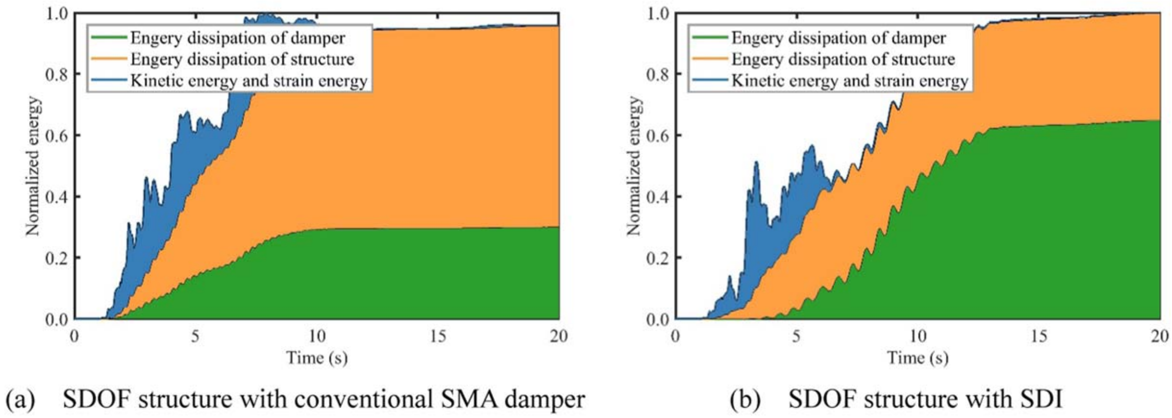

Figure 15. Normalized energy-time curves of SDOF structures installed with different SMA dampers.

tested, along with an original structure lacking either. The time history responses of all three displacements show that the SDI system reduces the structural displacement better than the conventional SMA damper, indicating that the structural vibration mitigation effect of an SMA element can be enhanced by an inerter element (figure 13).

The time history responses under all the acceleration records confirm that the SDI performs better than the conventional SMA damper with respect to structural acceleration mitigation (figure 14). In other words, more SMAs are required in a conventional SMA damper to achieve the same structural response mitigation effect as the SDI, resulting in higher material costs.

The normalized energy-time curves of the SDOF structures equipped with conventional SMA dampers and SDIs are classified into the energy dissipation of the damper and primary structure, along with kinetic and strain energy (figure 15). Most of the seismic energy is dissipated by the SDI, which performs better than the conventional SMA damper.

To further illustrate the enhanced energy dissipation capacity of an SMA element assisted by an inerter element, load-displacement curves of SMA elements in an SDI system

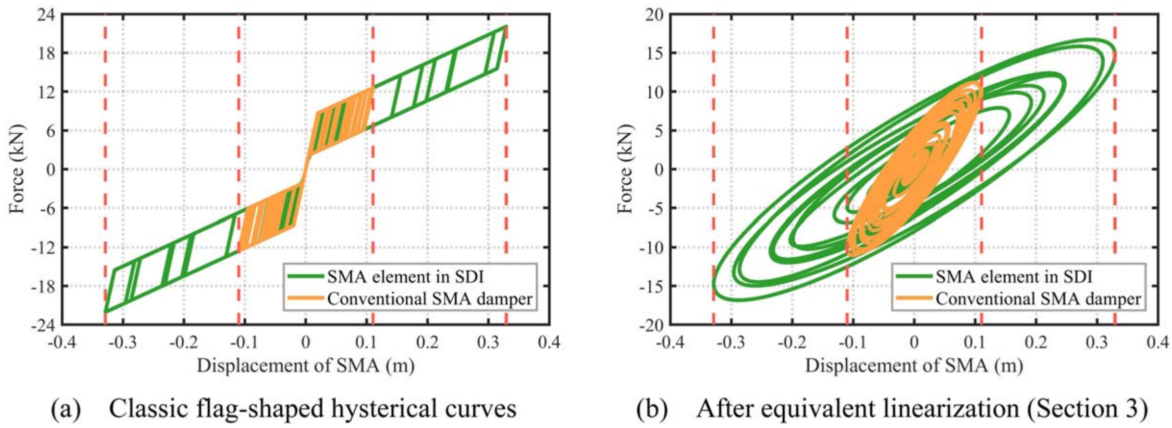

Figure 16. Load-displacement curves of SMA elements under the recorded ground motion GM3.

and a conventional SMA damper are calculated (figure 16). The deformation range of the SMA element clearly increases from 0.22 m in the conventional SMA damper to 0.66 m in the SDI, indicating that deformation could be enhanced significantly by the inerter element. This forms a more sufficient hysteresis loop, representing a superior capacity to dissipate seismic energy and mitigate structural vibration.

7. Conclusions

This study developed a novel SDI system in which the SMA and inerter elements are arranged in parallel and deployed in series with a linear supporting spring. After testing, the following conclusions can be drawn:

1. Compared to a conventional SMA damper, the new SDI system significantly improves the mitigation effect of structural displacement and acceleration due to seismic motions, indicating that a lower SMA material cost is needed in the design for the same structural response mitigation requirement.
2. The interactions of the SMA and inerter elements enlarge the deformation of the SMA element to enhance the SDI's ability to dissipate seismic energy; thus the potential of SMA material can by fully utilized by the introduction of an inerter element.
3. Fully combining the advantages of SMA's superelasticity and the inerter element's damping amplification effect, the SDI proposed here is a promising mechanism and can be regarded as a robust technology for structural vibration mitigation.
4. However, this study represents a preliminary test, so exploring the optimal performance of the SDI is of great significance in future research.

Acknowledgments

This research was supported by the National Natural Science Foundation of China (51978525 and 51778490), International Collaboration Program for Science and Technology, Commission of Ministry of Science and Technology, China (grant number 2016YFE0127600), Shanghai Pujiang Program (grant number 17PJ1409200), and Fundamental Research Funds for Central Universities of China (grant number 22120180064).

ORCID iDs

Yingqi Jia https://orcid.org/0000-0002-3541-5535
Lingzhi Li https://orcid.org/0000-0002-9477-6824
Chao Wang https://orcid.org/0000-0002-0347-7256
Ruifu Zhang https://orcid.org/0000-0003-2988-4412

References

[1] Asai T, Araki Y and Ikago K 2017 Structural control with tuned inertial mass electromagnetic transducers *Struct. Control Health* **25** e2059
[2] Asai T, Araki Y and Ikago K 2017 Energy harvesting potential of tuned inertial mass electromagnetic transducers *Mech. Syst. Signal Process.* **84** 659–72
[3] Pan C and Zhang R F 2018 Design of structure with inerter system based on stochastic response mitigation ratio *Struct. Control Health* **25** e2169
[4] Ikago K, Saito K and Inoue N 2012 Seismic control of single-degree-of-freedom structure using tuned viscous mass damper *Earthq. Eng. Struct. Dyn.* **41** 453–74
[5] Zhao Z P, Zhang R F and Lu Z 2019 A particle inerter system for structural seismic response mitigation *J. Franklin Inst.* (https://doi.org/10.1016/j.jfranklin.2019.02.001)
[6] Hieu D V, Hai N Q and Hung D T 2018 The equivalent linearization method with a weighted averaging for solving undamped nonlinear oscillators *J. Appl. Math.* **2018** 7487851
[7] Li R, Ge H and Shu G 2018 Parametric study on seismic control design of a new type of SMA damper installed in a frame-type bridge pier *J. Aerospace Eng.* **31** 4017100
[8] Huang H and Chang W 2018 Application of pre-stressed SMA-based tuned mass damper to a timber floor system *Eng. Struct.* **167** 143–50
[9] Wang B and Zhu S 2018 Superelastic SMA U-shaped dampers with self-centering functions *Smart Mater. Struct.* **27** 55003
[10] Mishra S K, Gur S and Chakraborty S 2013 An improved tuned mass damper (SMA-TMD) assisted by a shape memory alloy spring *Smart Mater. Struct.* **22** 95016

[11] Ikago K, Sugimura Y, Saito K and Inoue N 2012 Modal response characteristics of a multiple-degree-of-freedom structure incorporated with tuned viscous mass dampers *J. Asian Archit. Build.* **11** 375–82
[12] Zhang R F, Wang C, Pan C, Shen H, Ge Q Z and Zhang L Q 2018 Simplified design of elastoplastic structures with metallic yielding dampers based on the concept of uniform *Eng. Struct.* **176** 734–45
[13] Parulekar Y M, Ravi Kiran A, Reddy G R, Singh R K and Vaze K K 2014 Shake table tests and analytical simulations of a steel structure with shape memory alloy dampers *Smart Mater. Struct.* **23** 125002
[14] Qian H, Li H and Song G 2016 Experimental investigations of building structure with a superelastic shape memory alloy friction damper subject to seismic loads *Smart Mater. Struct.* **25** 125026
[15] Jiang C J, Lu Z D and Li L Z 2017 Shear performance of fire-damaged reinforced concrete beams repaired by a bolted side-plating technique *J. Struct. Eng.* **143** 4017007
[16] Jiang C J, Lu Z D, Li L Z and Liu B Z 2017 Experimental study on shear performance of bolted-side plated strengthening fire-damaged reinforced concrete beams *J. Build. Struct.* **38** 67–75
[17] Barbieri M, Ilanko S and Pellicano F 2018 Active vibration control of seismic excitation *Nonlinear Dyn.* **93** 41–52
[18] Xu L, Yu Y and Cui Y 2018 Active vibration control for seismic excited building structures under actuator saturation, measurement stochastic noise and quantisation *Eng. Struct.* **156** 1–11
[19] Gonzalez-Buelga A, Clare L R, Neild S A, Jiang J Z and Inman D J 2015 An electromagnetic inerter-based vibration suppression device *Smart Mater. Struct.* **24** 55015
[20] Nakamura Y, Fukukita A, Tamura K, Yamazaki I, Matsuoka T, Hiramoto K and Sunakoda K 2014 Seismic response control using electromagnetic inertial mass dampers *Earthq. Eng. Struct.* D **43** 507–27
[21] Lu Z, Wang Z X, Masri S F and Lu X L 2018 Particle impact dampers: past, present, and future *Struct. Control Health* **25** e2058
[22] Hu R C, Xiong H, Jin W L and Zhu W Q 2016 Stochastic minimax semi-active control for MDOF nonlinear uncertain systems under combined harmonic and wide-band noise excitations using MR dampers *Int. J. Nonlinear Mech.* **83** 26–38
[23] Garrido H, Curadelli O and Ambrosini D 2018 On the assumed inherent stability of semi-active control systems *Eng. Struct.* **159** 286–98
[24] Love J S, Tait M J and Toopchi-Nezhad H 2011 A hybrid structural control system using a tuned liquid damper to reduce the wind induced motion of a base isolated structure *Eng. Struct.* **33** 738–46
[25] Li H N, Huang Z, Fu X and Li G 2018 A re-centering deformation-amplified shape memory alloy damper for mitigating seismic response of building structures *Struct. Control Health* **25** e2233
[26] Jia Y Q, Lu Z D, Li L Z and Wu Z L 2018 A review of applications and research of shape memory alloys in civil engineering *IOP Conf. Ser.: Mater. Sci. Eng.* **392** 22009
[27] Araki Y, Shrestha K C, Maekawa N, Koetaka Y, Omori T and Kainuma R 2016 Shaking table tests of steel frame with superelastic Cu–Al–Mn SMA tension braces *Earthq. Eng. Struct. Dyn.* **45** 297–314
[28] Araki Y, Maekawa N, Shrestha K C, Yamakawa M, Koetaka Y, Omori T and Kainuma R 2014 Feasibility of tension braces using Cu–Al–Mn superelastic alloy bars *Struct. Control Hlth.* **21** 1304–15
[29] Pan C, Zhang R F, Luo H, Li C and Shen H 2018 Demand-based optimal design of oscillator with parallel-layout viscous inerter damper *Struct. Control Health* **25** e2051
[30] Zhang R F, Zhao Z P and Dai K S 2019 Seismic response mitigation of a wind turbine tower using a tuned parallel inerter mass system *Eng. Struct.* **180** 29–39
[31] De Domenico D, Impollonia N and Ricciardi G 2018 Soil-dependent optimum design of a new passive vibration control system combining seismic base isolation with tuned inerter damper *Soil Dyn. Earthq. Eng.* **105** 37–53
[32] Javidialesaadi A and Wierschem N E 2018 Optimal design of rotational inertial double tuned mass dampers under random excitation *Eng. Struct.* **165** 412–21
[33] Ozbulut O E, Hurlebaus S and Desroches R 2011 Seismic response control using shape memory alloys: a review *J. Intell. Mater. Syst. Struct.* **22** 1531–49
[34] Reedlunn B, Churchill C B, Nelson E E, Shaw J A and Daly S H 2014 Tension, compression, and bending of superelastic shape memory alloy tubes *J. Mech. Phys. Solids* **63** 506–37
[35] Ma H and Cho C 2008 Feasibility study on a superelastic SMA damper with re-centring capability *Mater. Sci. Eng.* A **473** 290–6
[36] Brinson L C 1993 One-dimensional constitutive behavior of shape memory alloys: Thermomechanical derivation with non-constant material functions and redefined martensite internal variable *J. Intell. Mater. Syst. Struct.* **4** 229–42
[37] Du X W, Sun G and Sun S S 2005 Piecewise linear constitutive relation for pseudo-elasticity of shape memory alloy (SMA) *Mater. Sci. Eng.* A **393** 332–7
[38] Graesser E J and Cozzarelli F A 1991 Shape memory alloys as new materials for seismic isolation *J. Eng. Mech.* **117** 2590–608
[39] Wen Y K 1980 Equivalent linearization for hysteretic systems under random excitation *J. Appl. Mech.* **47** 150–4
[40] Yan X and Nie J 2000 Response of SMA superelastic systems under random excitation *J. Sound Vib.* **238** 893–901
[41] Wang R, Yasuda K and Zhang Z 2000 A generalized analysis technique of the stationary FPK equation in nonlinear systems under Gaussian white noise excitations *Int. J. Eng. Sci.* **38** 1315–30
[42] De Lataillade A, Blanco S, Clergent Y, Dufresne J L, El Hafi M and Fournier R 2002 Monte Carlo method and sensitivity estimations *J. Quant. Spectrosc. Radiat. Transfer* **75** 529–38
[43] Zhu W Q, Huang Z L and Suzuki Y 2001 Equivalent nonlinear system method for stochastically excited and dissipated partially integrable Hamiltonian systems *Int. J. Nonlinear Mech.* **36** 773–86
[44] Rofooei F R, Mobarake A and Ahmadi G 2001 Generation of artificial earthquake records with a nonstationary Kanai–Tajimi model *Eng. Struct.* **23** 827–37
[45] Chopra A K 2007 *Dynamics of Structures: Theory and Applications to Earthquake Engineering* 3rd edn (Upper Saddle River, NJ: Prentice Hall)
[46] Pan C, Zhang R F, Luo H and Shen H 2016 Baseline correction of vibration acceleration signals with inconsistent initial velocity and displacement *Adv. Mech. Eng.* (https://doi.org/10.1177/1687814016675534)
[47] Pan C, Zhang R F, Luo H and Shen H 2018 Target-based algorithm for baseline correction of inconsistent vibration signals *J. Vib. Control* **24** 2562–75